In vivo genetic dissection of O_2-evoked cGMP dynamics in a *Caenorhabditis elegans* gas sensor

Africa Couto[a], Shigekazu Oda[a], Viacheslav O. Nikolaev[b], Zoltan Soltesz[a], and Mario de Bono[a,1]

[a]Medical Research Council Laboratory of Molecular Biology, Cambridge CB2 0QH, United Kingdom; and [b]Emmy Noether Group of the Deutsche Forschungsgemeinschaft, Department of Cardiology and Pneumology, Georg August University Medical Center, D-37075 Göttingen, Germany

Edited by Paul W. Sternberg, California Institute of Technology, Pasadena, CA, and approved July 16, 2013 (received for review October 20, 2012)

cGMP signaling is widespread in the nervous system. However, it has proved difficult to visualize and genetically probe endogenously evoked cGMP dynamics in neurons in vivo. Here, we combine cGMP and Ca^{2+} biosensors to image and dissect a cGMP signaling network in a *Caenorhabditis elegans* oxygen-sensing neuron. We show that a rise in O_2 can evoke a tonic increase in cGMP that requires an atypical O_2-binding soluble guanylate cyclase and that is sustained until oxygen levels fall. Increased cGMP leads to a sustained Ca^{2+} response in the neuron that depends on cGMP-gated ion channels. Elevated levels of cGMP and Ca^{2+} stimulate competing negative feedback loops that shape cGMP dynamics. Ca^{2+}-dependent negative feedback loops, including activation of phosphodiesterase-1 (PDE-1), dampen the rise of cGMP. A different negative feedback loop, mediated by phosphodiesterase-2 (PDE-2) and stimulated by cGMP-dependent kinase (PKG), unexpectedly promotes cGMP accumulation following a rise in O_2, apparently by keeping in check gating of cGMP channels and limiting activation of Ca^{2+}-dependent negative feedback loops. Simultaneous imaging of Ca^{2+} and cGMP suggests that cGMP levels can rise close to cGMP channels while falling elsewhere. O_2-evoked cGMP and Ca^{2+} responses are highly reproducible when the same neuron in an individual animal is stimulated repeatedly, suggesting that cGMP transduction has high intrinsic reliability. However, responses vary substantially across individuals, despite animals being genetically identical and similarly reared. This variability may reflect stochastic differences in expression of cGMP signaling components. Our work provides in vivo insights into the architecture of neuronal cGMP signaling.

The second messenger cyclic guanosine monophosphate (cGMP) regulates a range of physiological processes. In nervous systems, it can transduce sensory inputs (1) and modulate neuronal excitability and learning (2) and is implicated in control of mood and cognition (3). Precise regulation of cGMP levels ([cGMP]) is thought critical for these functions. This importance has prompted development of genetically encoded cGMP indicators, with the goal of visualizing cGMP dynamics with high temporal and spatial resolution (4, 5). Although these sensors have been used to image pharmacologically evoked changes in cGMP in cultured cells or tissue slices (6–10), endogenous cGMP dynamics have not been visualized and functionally dissected in vivo in any nervous system (4, 5).

Local [cGMP] reflects the net activity of guanylate cyclases (GCs) that synthesize cGMP (11) and phosphodiesterases (PDEs) that degrade it (12, 13). Mammals have several families of GCs (14, 15) and eight families of cGMP PDEs (16), each with distinct regulatory properties. Different PDE types are often coexpressed, but little is known about how they work together. cGMP signaling alters cell physiology by controlling cGMP-dependent protein kinases (PKG) (17, 18), cGMP-gated channels (CNGC) (19), and cGMP-regulated PDEs (12). These cGMP effectors can also feed back to control cGMP dynamics.

cGMP is a major second messenger in *Caenorhabditis elegans*, implicated in the function of a third of its sensory neurons, including thermosensory, olfactory, gustatory, and O_2-sensing neurons (20). Genetic and behavioral studies suggest that cGMP mediates sensory transduction in many of these neurons (21–25). Despite this pervasiveness, cGMP has not been visualized in any *C. elegans* cell: genetic inferences about its roles in signal transduction are untested, and we have no mechanistic insights into cGMP signaling dynamics and feedback control. Consistent with the prominence of cGMP signaling in the nematode, the *C. elegans* genome encodes 34 GCs (26), six PDE genes, at least one PKG (24, 27, 28), and six CNGC subunits (19, 21, 22, 29–31).

Here, we use cGMP and Ca^{2+} sensors to visualize and dissect cGMP signaling dynamics in a *C. elegans* O_2 sensor. We image single and double mutants defective in a soluble guanylate cyclase (sGC), CNGC subunits, PDE-1, PDE-2, and PKG. Our results reveal a signaling network of interwoven checks and balances. Counterintuitively, cGMP activation of PDE-2 promotes cGMP accumulation by controlling gating of CNGC and limiting Ca^{2+}-mediated negative feedback, including activation of PDE-1. We show that cGMP signal transduction is highly reliable when the same individual is stimulated repeatedly but, surprisingly, is highly variable across genetically identical, similarly reared animals. Finally, simultaneous imaging of O_2-evoked cGMP and Ca^{2+} responses suggests that cGMP dynamics can differ in distinct subcellular compartments of a *C. elegans* neuron, consistent with the existence of cGMP nanodomains.

Results

In Vivo Imaging of O_2-Evoked cGMP Responses in PQR and AQR Neurons. Several cGMP sensors based on Förster resonance energy transfer (FRET) have been developed that report cGMP changes in real time. These sensors vary in their dynamics, binding affinity, and cyclic-nucleotide specificity (4). We fused cDNA encoding three of the sensors to the *gcy-37* promoter, to drive expression in the AQR, PQR, and URX O_2-sensing neurons. Two

Significance

Although cGMP is a prominent second messenger in neurons, it has proven difficult to follow its dynamics in an intact nervous system in real time. Here, we use a genetically encoded cGMP sensor, cGi500, to visualize and genetically dissect endogenous cGMP dynamics in vivo. As a model, we use a *Caenorhabditis elegans* O_2-sensing neuron. We uncover mutually regulating negative feedback mechanisms mediated by cGMP and Ca^{2+} that involve PDE-1 and PDE-2 phosphodiesterases, protein kinase G, and cyclic nucleotide-gated channels. By simultaneously imaging Ca^{2+} and cGMP, we provide evidence of compartmentalization of cGMP signaling in different cellular domains.

Author contributions: A.C., S.O., V.O.N., Z.S., and M.d.B. designed research; A.C., S.O., V.O.N., and Z.S. performed research; A.C., S.O., V.O.N., and Z.S. analyzed data; and A.C. and M.d.B. wrote the paper.

The authors declare no conflict of interest.

This article is a PNAS Direct Submission.

Freely available online through the PNAS open access option.

[1]To whom correspondence should be addressed. E-mail: debono@mrc-lmb.cam.ac.uk.

This article contains supporting information online at www.pnas.org/lookup/suppl/doi:10.1073/pnas.1217428110/-/DCSupplemental.

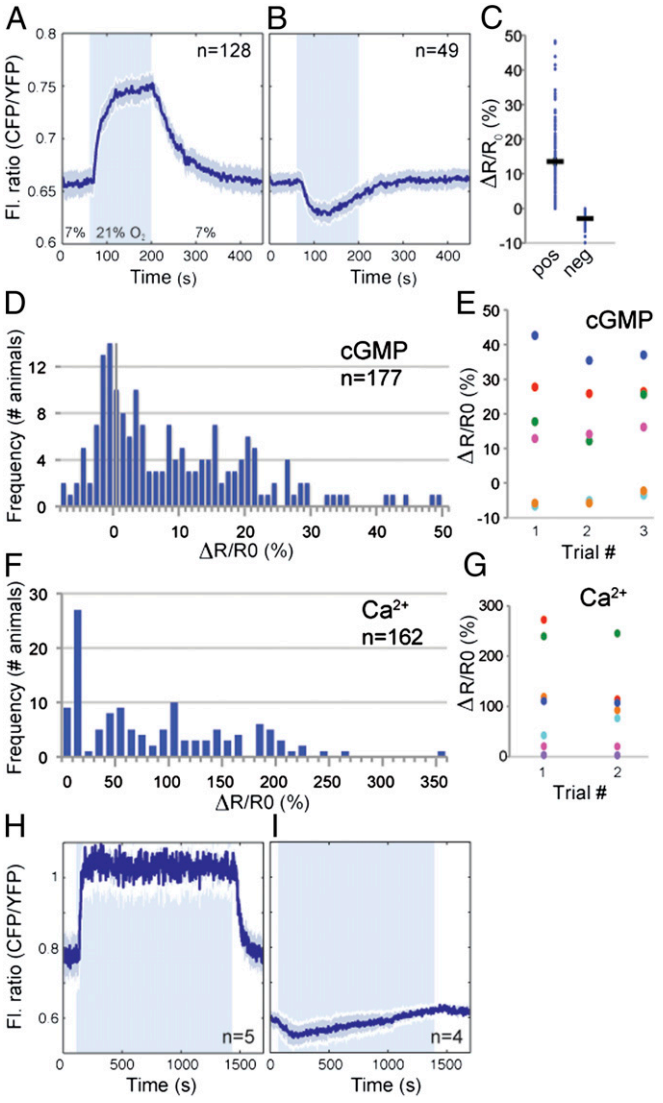

Fig. 1. O_2-evoked cGMP dynamics in PQR. (*A* and *B*) Average fluorescence ratio (CFP/YFP) changes evoked by a 7%–21%–7% O_2 stimulus in PQR neurons expressing cGi500. (*A*) In 72% of animals, the sensor reports an increase in [cGMP] when [O_2] rises to 21%. (*B*) In 28% of animals, it reports a decrease. In this and all figures, *n* = number of animals assayed, and the blue area indicates when [O_2] was 21%. The solid line shows the average ratio and the shading around it the SEM. The fluorescence ratio is plotted as CFP/YFP for convenience: an increase in this ratio indicates an increase in [cGMP]. (*C*) Quantification of the responses in *A* and *B*. R_o is the mean fluorescence ratio at 7% O_2 measured in the 30 s before the switch to 21% O_2. R_f is the mean fluorescence ratio at 21% O_2, measured during the last 30 s at 21%. ΔR is $R_f - R_o$. In this and subsequent figures, each dot indicates one recording, and black bars indicate average $\Delta R/R_o \pm$ SEM. (*D*) Histogram showing interindividual variation in cGMP responses evoked in PQR by a 7%–21% rise in O_2. The *y* axis is frequency of occurrence. (*E*) Scatter plot comparing inter- and intraindividual variation in cGMP responses evoked by repeated stimulation with a 7%–21% rise in O_2. Each color represents one animal. The *x* axis indicates iterative stimulation. The 96.9% of the total variance is due to interindividual variation ($P < 0.0001$ ***); the remainder includes all other variation (two-way random effect ANOVA). (*F*) Histogram showing interindividual variation in Ca^{2+} responses evoked in PQR by a 7%–21% rise in O_2. Data are from immobilized animals. (*G*) Scatter plot comparing inter- and intraindividual variation in Ca^{2+} responses evoked by repeated stimulation with a 7%–21% rise in O_2 in freely moving animals. Each color represents one animal; the *x* axis indicates round of stimulation. The 88.5% of the total variance is due to interindividual variation ($P = 0.007$ **); the remainder includes all other sources of variation (two-way random effect ANOVA). (*H* and *I*) Average fluorescence ratio (CFP/YFP) traces during persistent exposure to 21% O_2. Sustained high [O_2] elicits tonic elevation of [cGMP] in PQR in the majority of animals (*H*). In a subset of individuals, cGMP levels fall and then gradually return to baseline after a switch from 7% to 21% O_2 (*I*).

sensors, cGES-DE2 and cGES-DE5 (32), expressed poorly or formed aggregates. By contrast, the cGi500 cGMP sensor based on cGMP kinase Iα (33) (Fig. S1*A*) showed diffuse, cytoplasmic fluorescence as expected for a soluble protein (Fig. S1*B*). cGi500 expression did not alter the anatomy of URX, AQR, and PQR (Fig. S1*B*) or disrupt O_2-evoked behavioral responses mediated by these neurons in animals defective in *npr-1* (neuropeptide receptor-1) (Fig. S1 *C* and *D*), suggesting that it did not compromise neuron function. In *npr-1* mutants, O_2-sensing neurons control locomotory activity according to ambient O_2 levels (34).

Binding of O_2 to an sGC consisting of GCY-35 (GCY, *g*uanylate *cy*clase) and GCY-36 is proposed to stimulate cyclase activity and raise [cGMP] in PQR (35–37). To visualize O_2-evoked cGMP responses, we exposed animals expressing *pgcy-37::cGi500* to a 7%–21%–7% O_2 cycle and measured fluorescence changes in the PQR cell body. A rise in [O_2] usually elicited a decrease in the YFP/CFP FRET ratio, as predicted for the cGi500 sensor if the stimulus led to a rise in [cGMP] (Fig. S1*E*). As expected for a FRET sensor, ratio changes reflected reciprocal variation in YFP and CFP emission intensities (Fig. S1*E*). For clarity, in subsequent traces, we have plotted CFP/YFP ratios because increases in this ratio correspond to increases in [cGMP] (Fig. 1*A*). The average response to a 7%–21% O_2 stimulus was 13.5% (Fig. 1 *A* and *C*), and the maximum response was reached within 2 min of stimulus onset (Fig. 1*A*). When [O_2] returned to 7%, [cGMP] fell back to baseline within 3 min (Fig. 1*A*). Thus, in most animals (72%, Fig. 1 *A, C,* and *D*), a rise in [O_2] evoked a rapid rise in [cGMP] in PQR, consistent with increasing [O_2] stimulating cGMP production.

Unexpectedly, in the remaining 28% of animals, the same O_2 shift evoked small but significant decreases in reported [cGMP] (Fig. 1 *B* and *D*). The average peak magnitude of these responses was −2.9% and occurred ∼1 min after the O_2 switch (Fig. 1 *B* and *C*). Like positive responses, negative responses reflected reciprocal changes in CFP and YFP fluorescence (Fig. S1*F*), suggesting that they reported genuine changes in [cGMP]. Responses of opposite signs did not reflect animal-to-animal variation in sensor expression: the magnitude of responses evoked by a 7%–21% O_2 change did not correlate with cGi500 levels (Fig. S1*G*) or with absolute FRET ratio at 7% [O_2] (Fig. S1*H*). However, because high sensor expression might buffer cGMP, throughout our study, we imaged animals with similar and intermediate sensor levels.

To extend our study and further test cGi500 use in *C. elegans* neurons, we imaged O_2-evoked responses in the AQR neuron. The responses we obtained were similar to those we saw in PQR: a 7%–21% rise in O_2 could evoke either a rise or a fall in cGMP (Fig. S1 *I–K*).

Reliability of O_2-Evoked cGMP Signaling. We were surprised that the same O_2 stimulus evoked cGMP responses of opposite signs in both AQR and PQR in genetically identical animals grown under standard conditions. To explore this observation further, we examined cGMP responses in PQR in animals subjected to repeated cycles of a 7%–21%–7% O_2 stimulus. The sign and shape of cGMP responses evoked in PQR in an individual animal were highly reproducible across trials (Fig. 1*E* and Fig. S2 *A* and *B*). Of the total variance, 96.9% reflected interindividual differences; only 3.1% was due to intraindividual variation plus other sources of variation. Thus, cGMP signal transduction in PQR is highly reliable within an individual but varies across animals.

To extend our analysis, we examined intertrial variation in the Ca^{2+} responses evoked in PQR by the same 7%–21% O_2 switch, using a *pgcy-32::YC3.60* cameleon transgene. The magnitude and

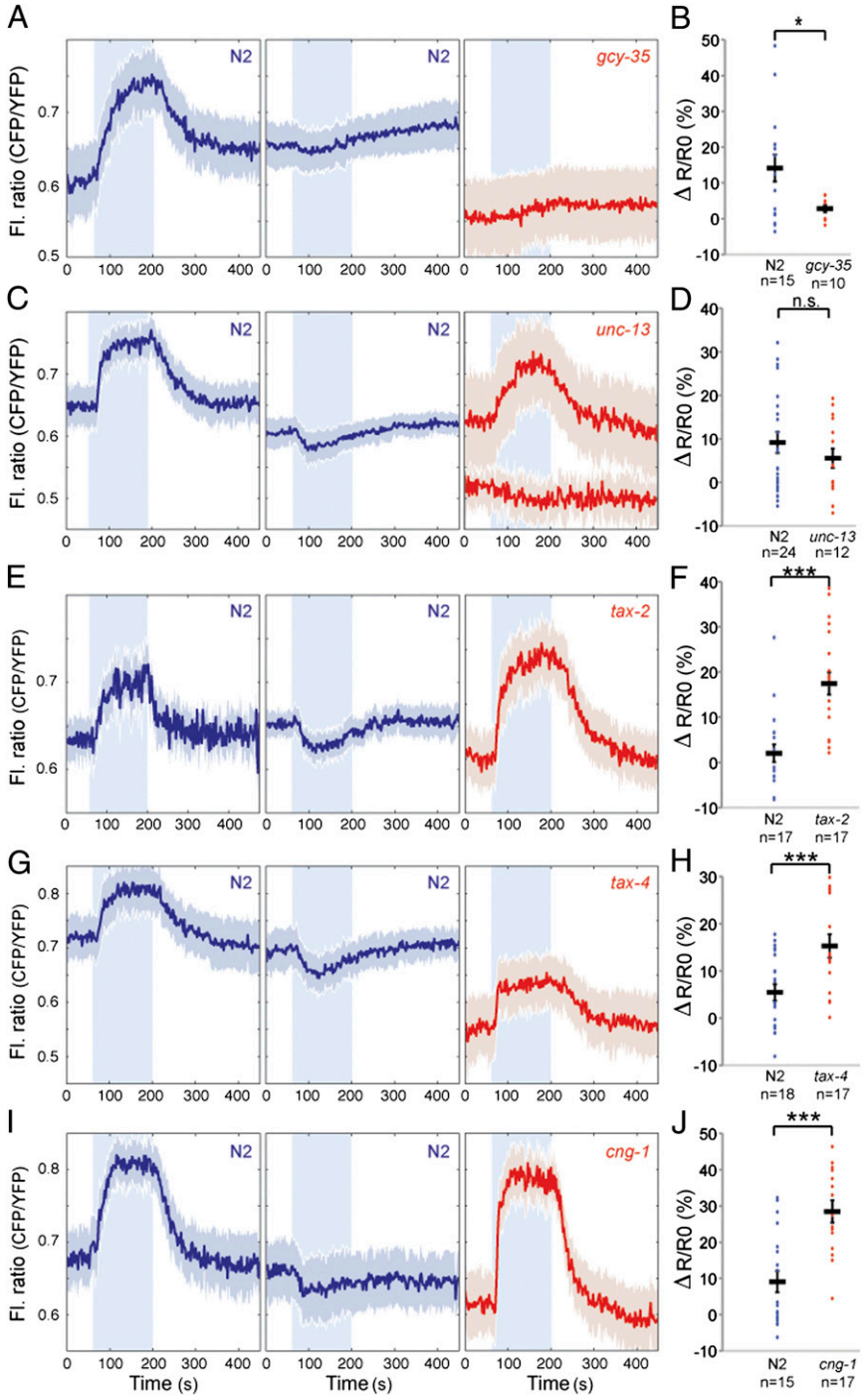

Fig. 2. cGMP-gated channel activity limits accumulation of cGMP. (*A*) Disrupting the *gcy-35* soluble guanylate cyclase abolishes O_2-evoked cGMP responses in PQR. In this and subsequent figures, traces from N2 control animals imaged in parallel are in blue, with negative and positive responses separated into two average traces. Traces from mutants are in red with genotype indicated. Because *gcy-35* mutants show no O_2-evoked response in PQR, only a single average trace is shown. (*B*) Quantification of the response amplitude from *A*. *gcy-35* mutant animals show no O_2-evoked cGMP responses. n.s., not significant; ***$P <$ 0.001; **$P < 0.01$, *$P < 0.05$ (two-tailed Student *t* test), in this and subsequent figures. (*C*) Average cGMP traces recorded in PQR for N2 and *unc-13* mutants. (*D*) The amplitude of cGMP responses in PQR of *unc-13* mutants is not significantly different from that of N2 animals. Like N2 animals, *unc-13* mutants exhibit occasional falls in cGMP following a rise in O_2. (*E*, *G*, and *I*) O_2-evoked cGMP responses in PQR in mutants defective in the TAX-2 cGMP-gated channel β subunit (*E*), and the TAX-4 (*G*) and CNG-1 (*I*) α subunits. (*F*, *H*, and *J*) Quantification of the responses in *E*, *G*, and *I*, respectively. Trace amplitudes in channel subunit mutants are significantly larger than in wild type, and negative responses are absent.

shape of Ca^{2+} responses varied substantially across isogenic, identically reared individuals (Fig. 1*F*). Moreover, 28% of animals showed a response amplitude of less than 10% and a lack of anticorrelation between CFP and YFP fluorescence changes. These results suggest that, in a quarter of animals, a 7%–21% O_2 shift failed to evoke a Ca^{2+} response in PQR.

To compare inter- and intraanimal variation in O_2-evoked Ca^{2+} responses in PQR, we stimulated freely moving animals twice

with a 7%–21% O_2 shift. We used freely moving animals to minimize animal handling. To control for variation introduced by the protocol, when imaging an animal for the second time, we repeated the set-up sequence as if imaging a new animal. ANOVA indicated that 88.5% of the total variance reflected interindividual differences (Fig. 1*G*); 11.5% included all other sources of variance (Fig. 1*G*). These data mirror the cGMP imaging results: signal transduction in PQR is highly reliable in an individual but varies across individuals, presumably due to difference in PQR signaling state.

High [O_2] Evokes Sustained Increases in [cGMP] in PQR. Ca^{2+} imaging indicates that PQR signals continuously at high [O_2] (38). Sustained signaling involves a relay of cGMP-gated channels, L-type voltage-gated Ca^{2+} channels, inositol 1,4,5-trisphosphate (IP_3) and ryanodine receptors. Relay activity is tightly coupled to [O_2]: a drop in [O_2] evokes a rapid drop in [Ca^{2+}] (34). To examine whether these properties reflected tonic control of [cGMP] by O_2, we exposed animals to a 7%–21%–7% O_2 stimulus but kept them at 21% O_2 for 20 min while imaging cGMP. Animals that responded with a rise in cGMP retained elevated [cGMP] as long as [O_2] was 21%, and [cGMP] promptly fell to baseline when [O_2] returned to 7% (Fig. 1*H*). In animals where the shift to 21% O_2 evoked a drop in [cGMP], this initial decrease was followed by a slow rise that returned [cGMP] to baseline (Fig. 1*I*). We detected no significant fluctuation in cGMP in PQR when animals were kept at 7% O_2 for 20 min. These data indicate that [O_2] can tonically regulate [cGMP] in PQR and that, following a rise in [O_2], increases in [cGMP] are stable over time.

O_2-Evoked Changes in PQR [cGMP] Require GCY-35 but Not Synaptic Input. We examined whether O_2-evoked cGMP responses in PQR required the *gcy-35* sGC. In *gcy-35* deletion mutants expressing the *pgcy-37::cGi500* transgene, the FRET ratio in PQR was unresponsive to changing [O_2] and was at values similar to those observed in wild-type animals held at 7% O_2 (Fig. 2 *A* and *B*). Thus, GCY-35 is necessary for measurable O_2-evoked cGMP signaling in PQR. The loss of positive and negative FRET responses in *gcy-35* mutants suggests that both reflect O_2-evoked changes in [cGMP].

To investigate whether O_2-evoked cGMP responses in PQR required synaptic input, we monitored cGMP responses in *unc-13* mutants, which are defective in synaptic release (39). FRET responses in *unc-13* mutants resembled wild-type controls after a 7%–21% O_2 switch (Fig. 2 *C* and *D*), suggesting that synaptic input into PQR does not strongly influence cGMP signaling.

Ca^{2+}-Dependent Negative Feedback Loops Cause O_2-Evoked Decreases in [cGMP]. A simple explanation for why rising O_2 can elicit either an increase or a decrease in [cGMP] in PQR is that high [O_2] activates not only cGMP production but also cGMP degradation, via negative feedback loops. One such feedback signal could be an increase in [Ca^{2+}] following gating of CNGC and subsequent opening of L-type voltage-gated Ca^{2+} channels, IP_3 and ryanodine receptors. In this model, variation in Ca^{2+} entry helps explain variation in cGMP accumulation in the cell body. This hypothesis predicts that disrupting Ca^{2+} entry should eliminate negative cGMP responses and increase the magnitude of positive ones. PQR expresses at least three cGMP-gated ion channel subunits—the chemotaxis abnormal (TAX)-4 and CNG-1 α subunits, and the TAX-2 β subunit (20, 21). Mutating any of these three subunits disrupts the Ca^{2+} influx evoked by a 7%–21% rise in [O_2] (36, 37). In *tax-2*, *tax-4*, or *cng-1* loss-of-function mutants, we never observed a decrease in [cGMP] in PQR in response to a 7%–21% O_2 stimulus (Fig. 2 *E*–*J*). Moreover, O_2-evoked [cGMP] responses were significantly larger in these mutants than in wild-type controls. These data support the notion that Ca^{2+} influx following gating of CNGCs stimulates negative feedback loops that limit cGMP accumulation in PQR.

Simultaneous Imaging of cGMP and Ca^{2+} Responses Suggests Compartmentalization of cGMP Signaling in PQR. To probe the relationship between Ca^{2+} and cGMP when a rise in O_2 evoked a fall in cGMP, we simultaneously imaged both messengers by combining the cGi500 cGMP reporter with the spectrally distinct R-GECO1 (red intensiometric genetically encoded Ca2+-indicator for optical imaging) Ca^{2+} indicator (40) (*Materials and Methods*). We found that negative cGMP responses were invariably associated with a concurrent sharp rise in Ca^{2+} in the cell body of PQR (Fig. 3). In cases where PQR did not show a Ca^{2+} response, we also failed to see changes in [cGMP]. These data are consistent with negative cGMP responses being due to Ca^{2+}-mediated negative feedback mechanisms. They also imply that different parts of PQR can have distinct cGMP dynamics because O_2-evoked Ca^{2+} increases in PQR require the gating of CNGC by binding of cGMP. To explain our data, we propose a model where cGMP rises at the membrane in the vicinity of the prenylated soluble guanylate cyclases and the cGMP-gated ion channels, but occasionally falls in the cell body due to strong cytosolic Ca^{2+}-mediated negative feedback loops.

***C. elegans* PDE-1 is a Ca^{2+}-Activated Dual Specificity cGMP/cAMP PDE and Participates in a Negative Feedback on [cGMP].** One of the six PDEs in *C. elegans*, PDE-1, is orthologous to PDE1, the mammalian Ca^{2+}/calmodulin-dependent PDE, and could contribute to Ca^{2+}-mediated negative feedback on cGMP accumulation. In genetic screens for mutations that disrupted O_2-evoked *C. elegans*

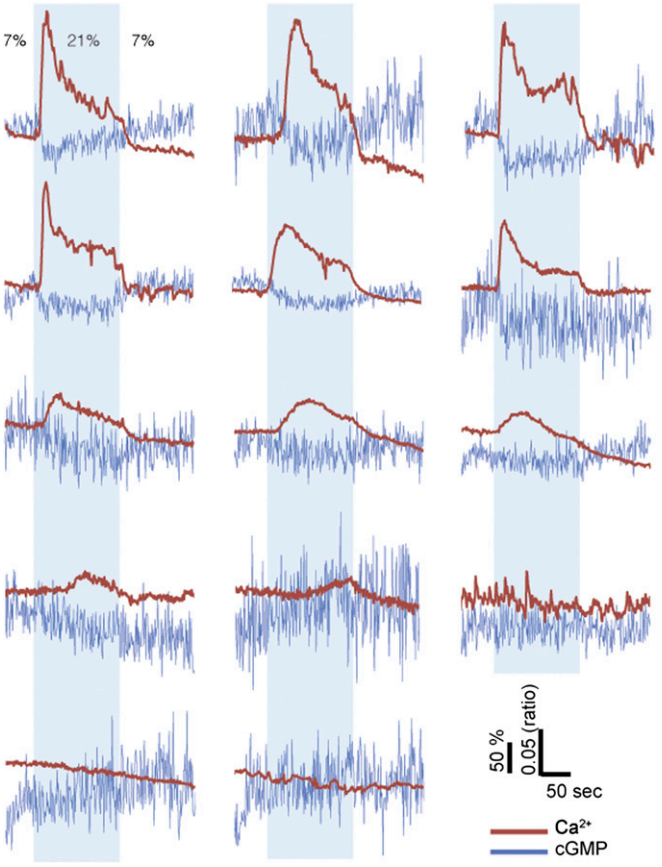

Fig. 3. Simultaneous imaging of Ca^{2+} and cGMP. Traces for individual animals showing simultaneous imaging of Ca^{2+} and cGMP responses evoked by a 7%–21%–7% O_2 stimulus train. Ca^{2+} responses are measured using R-GECO1. cGMP responses are measured using cGi500. Scales for responses are shown bottom right as % fluorescence change ΔR/Ro (R-GECO1) and CFP/YFP fluorescence ratio (cGi500).

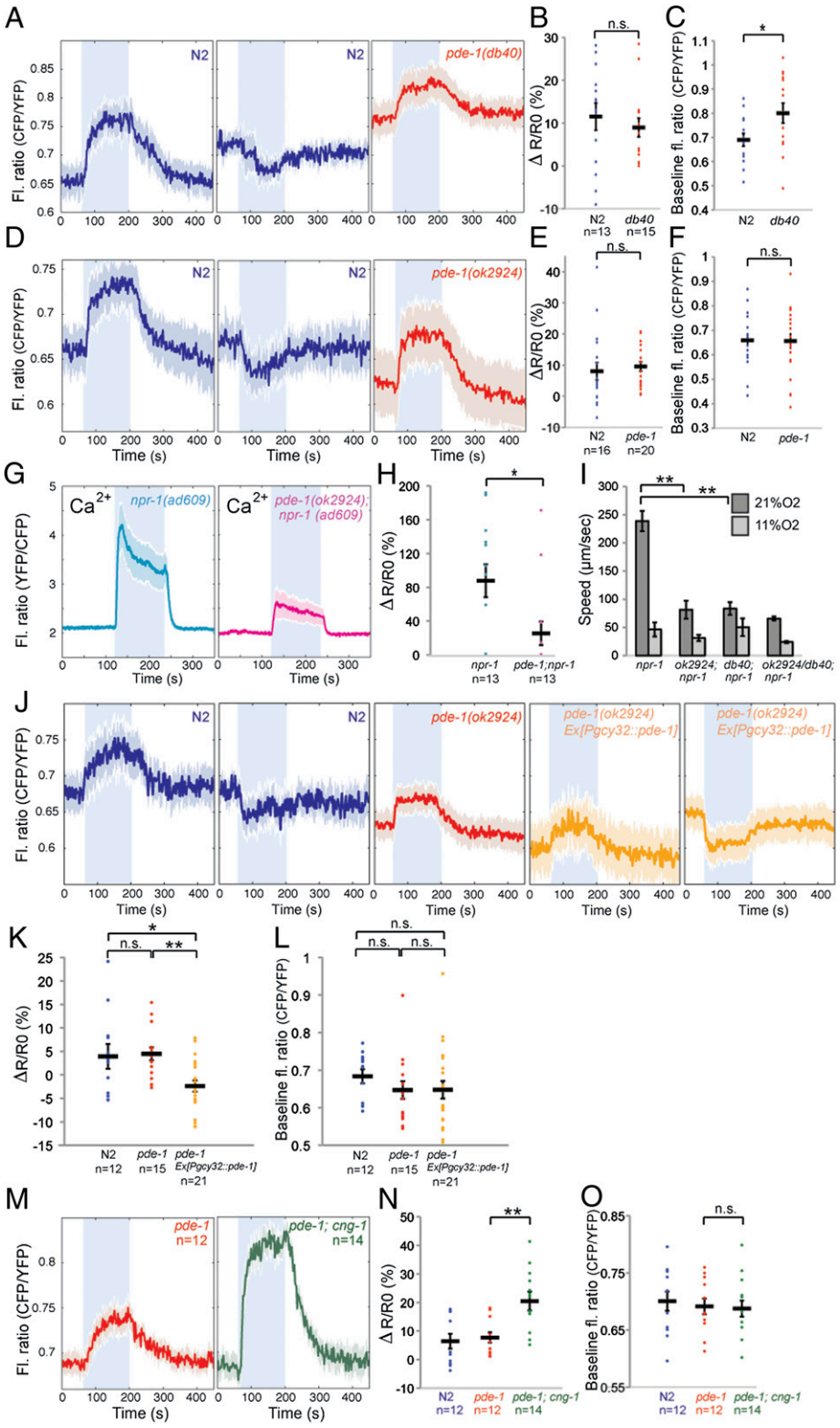

Fig. 4. PDE-1 mediated negative feedback. (*A* and *D*) Average cGMP traces in PQR of *pde-1(db40)* (*A*) and *pde-1(ok2924)* (*B*) mutants compared with N2 controls. Disrupting *pde-1* eliminates negative cGMP responses to a rise in $[O_2]$. (*B* and *E*) Quantification of the amplitude of cGMP traces for *pde-1* (*db40)* (*B*) and *ok2924* allele (*E*) compared with wild type. (*C* and *F*) Comparison of [cGMP] in *pde-1* mutants and wild type when animals are kept at 7% O_2. In this and subsequent panels, this value is measured by averaging the baseline CFP/YFP fluorescence ratio during the 30 s before the switch to 21% O_2. (*G* and *H*) Comparison of O_2-evoked average Ca^{2+} responses in PQR in *pde-1; npr-1* mutants and *npr-1* controls (*G*). Individual responses are plotted in *H*. (*I*) *pde-1; npr-1* animals show reduced locomotory activity at 21% O_2 compared with control *npr-1* animals. (*J–L*) Average cGMP traces in PQR of *pde-1(ok2924)* mutants overexpressing a *pgcy-32::pde-1* cDNA transgene compared with nontransgenic controls. The *gcy-32* promoter drives expression in PQR, AQR, and URX neurons. In *pde-1* overexpressing animals, a rise in $[O_2]$ often elicits a drop in cGMP. (*M–O*) Negative feedback through *pde-1* only partly accounts for increased O_2-evoked cGMP responses in *cng-1* mutants (*M*). $\Delta R/R_0$ values for individual traces are plotted in *N*. (*O*) Comparison of PQR [cGMP] in *pde-1* and *pde-1; cng-1* mutants with wild-type controls when animals are kept at 7% O_2.

behaviors, we identified an allele of *pde-1, pde-1(db40),* that was associated with an H373Y amino acid substitution (*Materials and Methods*). In mammalian PDE1, the residue equivalent to H373 chelates a Zn^{2+} ion essential for PDE activity (16, 41). *pde-1 (db40)* is therefore likely to be a strong hypomorphic or null allele. As expected if PDE-1 participated in Ca^{2+}-dependent negative feedback on cGMP signaling in PQR, we did not observe decreases in cGMP following a rise in O_2 in *pde-1(db40)* mutants (Fig. 4 *A–C*) or in a *pde-1* deletion mutant, *pde-1(ok2924)* (Fig. 4 *D–F*). Interestingly, for both *pde-1* alleles, the changes in [cGMP] evoked when $[O_2]$ increased from 7% to 21%, or decreased from 21% to 7% occurred as rapid as in wild type. Baseline [cGMP] at 7% O_2, reported by the absolute value of the CFP/YFP FRET ratio, was only slightly elevated in *pde-1(db40)* mutants compared

with controls ($P < 0.05$), and this elevation was not observed in *pde-1(ok2924)* mutants (Fig. 4 *A–F*). As well as implicating PDE-1 in negative feedback control of [cGMP], these data suggest that at least one other PDE degrades cGMP in PQR.

To investigate how loss of PDE-1 altered PQR excitability, we imaged O_2-evoked Ca^{2+} responses in *pde-1(ok2924)* mutants using yellow cameleon 3.60 (YC3.60). As expected from imaging cGMP, loss of *pde-1* did not significantly alter baseline [Ca^{2+}] in PQR in animals kept at 7% O_2, and the onset and offset of the Ca^{2+} responses evoked by a rise or fall in [O_2] remained rapid. However, the average magnitude of the Ca^{2+} increase evoked by a switch from 7% to 21% O_2 was reduced in *pde-1* mutants compared with wild type (Fig. 4 *G* and *H*). These results suggest that a compensatory mechanism mitigates the consequences of loss of PDE-1, to prevent hyperactivation of the neuron (see below). Consistent with the decrease in O_2-evoked Ca^{2+} responses in PQR, disrupting *pde-1* blunted the speed increase elicited in *npr-1* animals when O_2 rises from 7% to 21% (Fig. 4*I*) (38).

In vitro studies have shown that *C. elegans* PDE-1 binds Ca^{2+}/CaM (CaM, calmodulin), but did not examine whether this binding stimulated phosphodiesterase activity (42). To test for Ca^{2+} stimulation of PDE-1, we cotransfected human embryonic kidney 293A (HEK293A) cells with DNA expressing the cGi500 cGMP sensor and either PDE-1 or an empty vector as a negative control. We then stimulated cells with 50 μM sodium nitroprusside (SNP) to increase [cGMP], followed by 100 μM ATP to increase cytosolic [Ca^{2+}]. Both PDE-1 and vector-transfected cells responded to SNP with a rapid rise in [cGMP] (Fig. S3 *A* and *B*). However, whereas cells transfected with empty vector did not respond to ATP addition (Fig. S3 *A* and *E*), cells transfected with PDE-1 showed a rapid decrease in [cGMP] (Fig. S3 *B* and *E*), as expected if *C. elegans* PDE-1 were stimulated by a rise in [Ca^{2+}]. The decrease in [cGMP] could be reversed by adding the competitive PDE inhibitor 3-isobutyl-1-methylxanthine (IBMX). These data suggest that *C. elegans* PDE-1 is a Ca^{2+}-stimulated cGMP phosphodiesterase. Similar experiments using 100 nM isoproterenol to stimulate cAMP production and the Epac1 cAMP sensor (Fig. S3 *C–E*) indicated that, like mammalian PDE1, *C. elegans* PDE-1 is a Ca^{2+}-activated dual specificity cGMP/cAMP PDE.

PDE-1 Acts Cell-Autonomously in PQR to Limit cGMP Accumulation. To examine whether PDE-1 acts cell-autonomously in O_2-sensing neurons to shape cGMP responses, we asked whether expressing *pde-1* cDNA in these neurons restored O_2-evoked negative cGMP responses to *pde-1* mutant animals. A PQR-specific promoter is not available, but we could restrict *pde-1* expression to PQR, AQR, and URX neurons using the *gcy-32* promoter. The incidence of negative cGMP responses in PQR following a rise in O_2 was much higher in animals expressing the *pgcy-32::pde-1* transgene than in sibling controls lacking the coinjection marker (Fig. 4 *J–L*). These data are consistent with a cell-autonomous role for *pde-1* in PQR. They also suggest that potentiating PDE-1 negative feedback on cGMP, by overexpressing this gene, can induce a gain-of-function phenotype in which a rise in O_2 is much more likely to evoke a fall in cGMP in the cell body. These data support a role for PDE-1 in a negative feedback loop that limits cGMP accumulation following gating of cGMP channels.

Ca^{2+}-Stimulated Negative Feedback on [cGMP] by PDE-1–Independent Mechanisms. To investigate whether PDE-1 activation was the only mechanism by which O_2-evoked Ca^{2+} entry inhibited cGMP accumulation in PQR, we compared the cGMP responses of *pde-1* and *pde-1; cng-1* double mutants. Although the baseline [cGMP] reported by the cGi500 sensor at 7% O_2 was similar in the two strains, the magnitude of the cGMP response evoked by a 7%–21% O_2 shift was significantly larger in *pde-1; cng-1* mutants compared with *pde-1* animals (Fig. 4 *M–O*). Thus, *pde-1*–independent mechanisms also play important roles to inhibit cGMP accumulation in PQR following O_2-evoked Ca^{2+} entry.

PDE-2 Promotes cGMP Accumulation in PQR by Limiting Ca^{2+}-Mediated Negative Feedback. In *pde-1* mutants, [cGMP] in PQR decreased rapidly when [O_2] fell from 21% to 7%, suggesting that other PDEs can act in this neuron to terminate responses. PDE-2 is the *C. elegans* ortholog of mammalian PDE2, a dual specificity PDE. It includes one N-terminal GAF (found in cGMP-specific phosphodiesterases, adenylyl cyclases and FhlA) domain similar in sequence and position to GAF-B, the second of two GAF domains in mammalian PDE2 (Fig. S4). cGMP binding to GAF-B stimulates mammalian PDE2, leading to negative feedback (16).

To test whether PDE-2 modified cGMP dynamics in PQR, we compared cGMP responses evoked by a 7%–21%–7% O_2 stimulus in wild type and *pde-2(tm3098)* mutants. *pde-2(tm3098)* is a deletion mutant that has an altered reading frame upstream of the catalytic domain and is likely to be null. In *pde-2* mutants, a 7%–21% rise in [O_2] evoked either a drop or no significant change in [cGMP] (Fig. 5 *A* and *C*). Baseline [cGMP] in PQR at 7% O_2 was not significantly different in *pde-2* compared with wild type (Fig. 5 *A* and *C*). Thus, PDE-2, like PDE-1, regulates cGMP dynamics in PQR. Counterintuitively, however, PDE-2 promotes rather than inhibits cGMP accumulation following a rise in O_2. The distinct effects of *pde-1* and *pde-2* mutations on O_2-evoked cGMP dynamics suggest that these cGMP phosphodiesterases play different roles in PQR.

We speculated that PDE-2 promoted O_2-evoked cGMP accumulation in PQR by keeping in check the Ca^{2+}-mediated negative feedback loops that operate following gating of CNGCs. To test this hypothesis, we examined cGMP responses in *pde-2* mutants defective in *cng-1*. In *cng-1; pde-2* double mutants, a 7%–21% O_2 stimulus elicited strong increases in [cGMP] in PQR and no observable decreases in [cGMP] (Fig. 5 *F*, *G*, and *I*). These data support the notion that PDE-2 limits Ca^{2+}-mediated negative feedback on [cGMP] in wild-type animals, presumably through its PDE activity controlling the gating of CNGCs.

To investigate the role of *pde-2* in PQR signaling further, we compared O_2-evoked Ca^{2+} responses in PQR in wild type and *pde-2* mutants (Fig. 5 *D* and *E*). Baseline [Ca^{2+}] at 7% O_2 was slightly elevated in *pde-2* mutants, and, of 18 animals tested, 10 responded to a switch from 7% to 21% O_2 with a rapid rise in Ca^{2+} that promptly returned to baseline when [O_2] was returned to 7%. However, the remaining 8 *pde-2(−)* animals failed to respond to a rise in [O_2] with a detectable [Ca^{2+}] response. By contrast, only 2/15 wild-type controls imaged in parallel failed to respond. Thus, disrupting *pde-2*, like disrupting *pde-1* (Fig. 4 *G* and *H*), is associated with increased failure to evoke a Ca^{2+} response following a rise in O_2.

To test whether the fall in [cGMP] evoked in *pde-2* mutants by a rise in [O_2] reflected, at least in part, increased PDE-1 activity, we built *pde-1; pde-2* double mutant strains and imaged their O_2-evoked cGMP responses. The double mutants exhibited elevated [cGMP] in PQR at 7% O_2 and showed negligible changes in [cGMP] when we switched [O_2] between 7% and 21% (Fig. 5 *H–J*). These results indicate that both PDE-1 and PDE-2 breakdown cGMP in PQR. The absence of O_2-evoked decreases in [cGMP] in *pde-1; pde-2* mutants is consistent with negative cGMP responses reflecting excessive PDE-1 activity in *pde-2* mutants. Finally, although our results do not exclude that additional PDEs act in PQR, they suggest that such PDEs, if they exist, are not sufficient to regulate PQR cGMP dynamics.

PKG Works with PDE-2 to Promote cGMP Accumulation After a Rise in [O_2]. Besides modulating cGMP-gated channels and PDEs, cGMP regulates PKG. The *C. elegans* ortholog of PKG is *egl-4* (24, 27), which has previously been shown to be expressed in PQR (28). We examined whether a loss-of-function allele of *egl-4*, *egl-4*

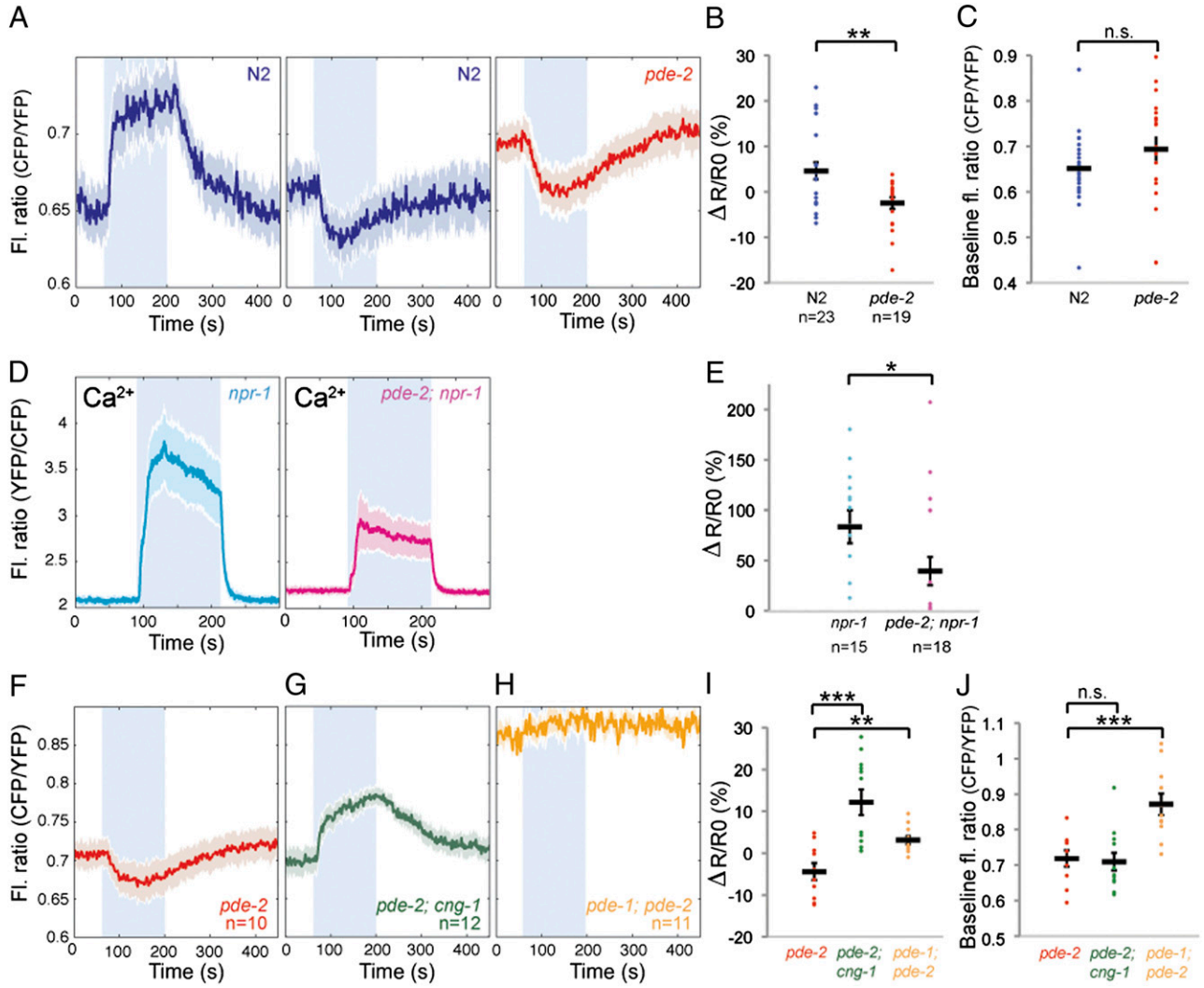

Fig. 5. PDE-2 promotes cGMP accumulation by limiting Ca^{2+}-dependent negative feedback. (*A*) Average O_2-evoked cGMP responses recorded from PQR in *pde-2(tm3098)* mutants compared with N2 controls. In *pde-2* mutants, a switch from 7% to 21% O_2 usually elicits a drop in [cGMP], unlike controls in which a rise in cGMP is usual. (*B* and *C*) Plot showing $\Delta R/R_0$ (*B*) and the baseline fluorescence ratio at 7% O_2 (*C*) for responses from *A*. (*D*) Average O_2-evoked Ca^{2+} responses in PQR in *pde-2(tm3098); npr-1(ad609)* mutants and *npr-1(ad609)* controls. Loss of *pde-2* reduces the average amplitude of Ca^{2+} responses evoked by 21% O_2. (*E*) Plot showing $\Delta R/R_0$ for individual Ca^{2+} responses from *D*. (*F–H*) Average O_2-evoked cGMP responses recorded from PQR in *pde-2, pde-2; cng-1* and *pde-1; pde-2* mutants. (*I* and *J*) Plot showing $\Delta R/R_0$ (*I*) and the baseline fluorescence ratio at 7% O_2 (*J*) for individual cGMP responses from *F*, *G*, and *H*.

(n478), disrupted O_2-evoked behaviors. *egl-4(n478); npr-1* double mutants moved slowly on food at 11% O_2, like *npr-1* animals. However, a switch to 21% O_2 evoked a much smaller increase in locomotory activity in *egl-4; npr-1* animals than *npr-1* controls (Fig. 6*A*). To investigate this further, we examined how disrupting *egl-4* altered Ca^{2+} and cGMP responses evoked in PQR by a 7%–21%–7% O_2 stimulus. Loss of *egl-4* slightly elevated the Ca^{2+} baseline at 7% O_2 and reduced the average Ca^{2+} response evoked by a 7%–21% O_2 stimulus (Fig. 6 *B* and *C*). This reduction partly reflected increased failure of O_2-evoked Ca^{2+} responses. Thus, the behavioral and the Ca^{2+} imaging phenotypes of *egl-4* mutants recapitulate those observed in *pde-2* mutants.

To investigate this similarity further, we imaged O_2-evoked cGMP responses in PQR. Like in *pde-2* mutants, a shift from 7% to 21% O_2 very often evoked a decrease in [cGMP] in *egl-4* mutants (compare Fig. 6 *D–F* with Fig. 5 *A–C*). *egl-4* mutants also showed higher [cGMP] at 7% O_2 compared with wild-type controls. We could rescue these *egl-4* cGMP phenotypes by expressing *egl-4* cDNA specifically in the AQR, PQR, and URX neurons, using the *gcy-36* promoter (Fig. 6 *G–I*), suggesting that they reflected cell-autonomous function of *egl-4* in PQR.

Like for *pde-2* mutants, the switch in the sign of the cGMP response in *egl-4* mutants was reversed in *egl-4; cng-1* double mutants (Fig. 6 *J, M,* and *N*). These results suggest that the O_2-evoked decreases in [cGMP] in *egl-4* mutants reflect Ca^{2+}-dependent negative feedback. Supporting this, disrupting the Ca^{2+}-activated PDE, *pde-1*, in *egl-4* mutants also prevented O_2-evoked decreases in [cGMP] and resulted in cGMP responses similar to those obtained in *egl-4; cng-1* and *pde-2; cng-1* double mutants (Fig. 6 *K, M,* and *N*). These data suggest that one role of EGL-4 PKG in PQR is to positively regulate PDE-2. This hypothesis predicts that the phenotypes of *pde-2* and *egl-4* would not be additive because they act together. Consistent with this, O_2-evoked cGMP responses in *pde-2; egl-4* animals resembled those of *pde-2* and *egl-4* single mutants (Fig. 6 *L–N*). These data suggest that PKG stimulates PDE-2 activity as cGMP rises. PKG-activated PDE-2 controls cGMP build-up and gating of CNGCs as O_2 rises, limiting Ca^{2+} entry and preventing excessive Ca^{2+}-mediated negative feedback on [cGMP].

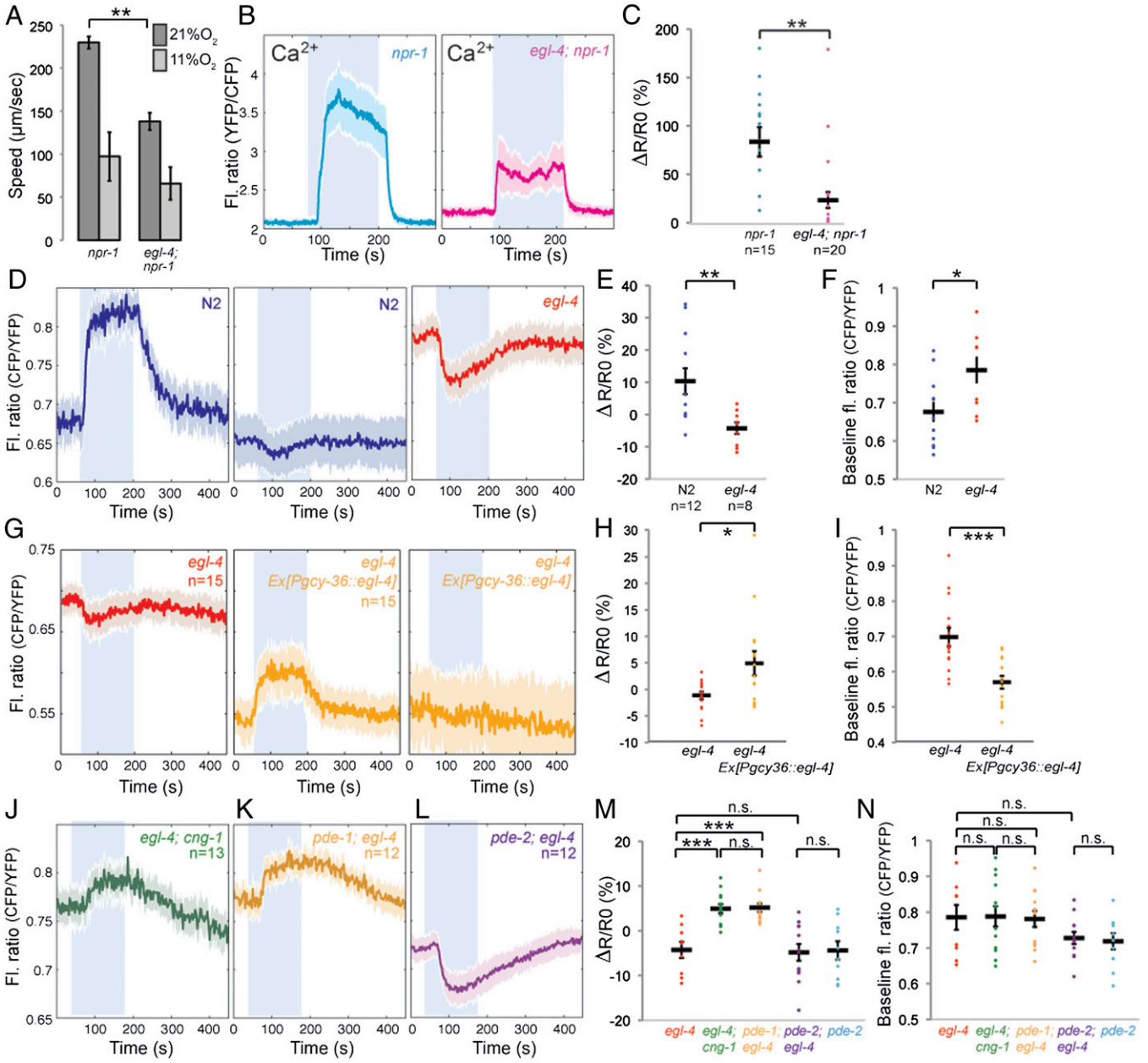

Fig. 6. PKG acts with PDE-2 to limit Ca^{2+}-dependent negative feedback on cGMP. (*A*) The *egl-4(n478)* loss-of-function allele reduces the locomotory activity of *npr-1* animals at 21% O_2. (*B* and *C*) *egl-4(n478)* reduces the Ca^{2+} influx evoked in PQR by a switch from 7% to 21% O_2. Average Ca^{2+} traces for *egl-4; npr-1* mutants and *npr-1* controls are shown in *B*. *C* shows the $\Delta R/R_0$ calculated from *B*. (*D–F*) *egl-4(n478)* increases PQR [cGMP] at 7% O_2 relative to wild type and leads predominantly to a fall in [cGMP] when O_2 rises from 7% to 21%. cGMP traces for *egl-4* mutants and N2 controls are shown in *D*. *E* shows the $\Delta R/R_0$ calculated from *D*. *F* shows the baseline fluorescence ratio at 7% O_2 for cGMP responses in *D*. (*G–I*) Reintroducing wild-type EGL-4 in *egl-4* mutant worms with a *pgcy36::egl-4* construct restores positive cGMP responses to a rise in O_2 and shifts down baseline cGMP levels at 7% O_2 in PQR. *G* shows average traces in *egl-4* nontransgenic (red) and transgenic (yellow) animals. *H* shows dR/R_0 from *G*, and *I* shows fluorescence ratio at 7% from *G*. (*J–L*) Disrupting *cng-1* (*J*) or *pde-1* (*K*) eliminates the negative cGMP responses elicited in *egl-4(n478)* mutants by a rise in [O_2] whereas disrupting *pde-2* does not (*L*). *M* shows the $\Delta R/R_0$ calculated for each individual included in *J–L*. *N* shows the baseline fluorescence ratio at 7% O_2 for individual cGMP responses from *J–L*.

Discussion

cGMP second messenger signaling is widespread in nervous systems, but direct visualization and genetic dissection of endogenous cGMP dynamics in neurons is lacking. Here, we image in vivo cGMP and Ca^{2+} dynamics in a genetically characterized system, the PQR O_2-sensing neuron in *C. elegans,* to gain insights into the relationships of different cGMP signaling components.

A striking feature of cGMP signaling is numerous PDEs, each with distinct regulatory properties (12, 13). Different PDEs are often coexpressed in the same neuron, but how they work together is poorly understood. *C. elegans* PDE-1 and PDE-2 are orthologs of mammalian Ca^{2+}-stimulated PDE1 and cGMP-stimulated PDE2, respectively. Our data suggest that these two PDEs can form mutually regulating negative feedback loops (Fig. 7). Our data suggest a model in which rising cGMP stimulates PKG and PDE-2, which feed back to dampen further cGMP increases. This brake attenuates gating of CNGCs, controls the rise in Ca^{2+}, and keeps in check Ca^{2+}-dependent negative feedback loops

that inhibit cGMP accumulation, including activation of PDE-1 (Fig. 7). Consistent with our model, negative cGMP responses are not observed in mutants defective in cGMP-gated channel subunits, and O_2-evoked cGMP responses are substantially bigger in such mutants. The scheme of balanced negative feedback loops that we propose may be widespread: in mammals, PDE1 and PDE2 are coexpressed in many brain areas, including cortex, hippocampus, and striatum (13). Moreover, PDE5, like PDE2, is stimulated by increases in cGMP (13) and activated by PKG, making interlocked PDE5–PDE-1 negative feedback loops an alternative possibility.

Our data also suggest that cGMP dynamics can differ in distinct compartments of the PQR neuron. Simultaneous imaging of cGMP and Ca^{2+} responses suggests that cGMP levels in the PQR cell body can fall while Ca^{2+} levels are rising sharply (Fig. 3). Because the Ca^{2+} response depends on gating of CNGCs, the simplest interpretation of these data is that cGMP rises locally in a juxtamembrane nanodomain close to the CNGC while falling in the cytoplasm. The sGCs GCY-35 and GCY-36 both have a C-terminal isoprenylation signal, and we have shown that the integrity of this signal is important for *gcy-35* transgenes to rescue *gcy-35* mutant phenotypes, suggesting that sGCs need to be at the membrane to stimulate channel activity (40). Both the sGC and the CNGC localize to the cilium of PQR although whether they interact directly is unclear (43, 44). The subcellular localization of PDE-1 and PDE-2 is unknown but may help explain how nanodomains with opposite cGMP dynamics can be set up. Note also that our model is likely simplified: we infer, but have not identified, additional Ca^{2+}-dependent negative feedback loops. These additional feedback mechanisms could involve any of a number of Ca^{2+} binding proteins encoded by the *C. elegans* genome, including neuronal Ca^{2+} sensors (NCS proteins), calcineurin, and Ca^{2+}/calmodulin-dependent kinases.

cGMP imaging shows that a rise in $[O_2]$ can trigger a rapid increase in [cGMP] in PQR that is sustained while $[O_2]$ is high, but falls when $[O_2]$ decreases. The rise in [cGMP] requires the O_2-binding atypical sGC GCY-35, suggesting that high $[O_2]$ tonically stimulates this cyclase in vivo. Tonic signaling in the AQR, PQR, and URX neurons can elicit long-lasting changes in *C. elegans* behavior (38). For example, *npr-1* animals move quickly as long as O_2 is at 21% but move slowly while O_2 remains at 7%. Intermediate O_2 tensions elicit intermediate behaviors (34). These graded behavioral responses mirror graded changes in the activity of O_2 sensors (38). Some of the negative feedback loops implicated in our study may help encode graded but persistent responses.

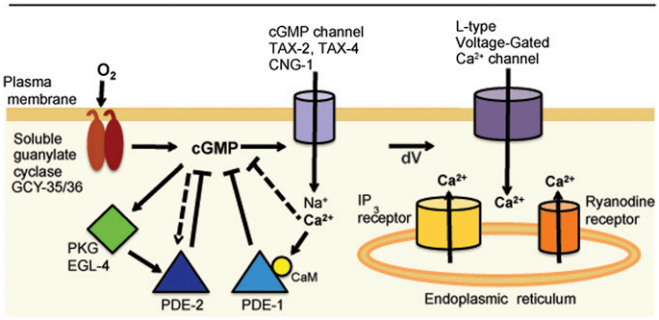

Fig. 7. Model for architecture of cGMP signaling in PQR. In our model, an $[O_2]$ increase persistently activates prenylated GCY-35/GCY-36 atypical soluble guanylate cyclases located at the membrane. The resulting increase in [cGMP] gates cGMP channels, promoting Na^+ and Ca^{2+} entry. The rise in [cGMP] and $[Ca^{2+}]$ stimulates competing negative feedback loops that sculpt signaling dynamics. In one loop, increasing [cGMP] stimulates EGL-4 PKG and activates PDE-2. By destroying cGMP, PKG–PDE-2 negative feedback acts as a smoothing filter, keeping in check CNGC gating. This control mechanism limits Ca^{2+}-dependent negative feedbacks on cGMP that are mediated by PDE-1 and PDE-1-independent mechanisms. Depolarization caused by sustained gating of CNGC activates L-type voltage-gated Ca^{2+} channels and leads to Ca^{2+} release from intracellular stores via ryanodine and IP_3 receptors, and sustained signaling. A fall in O_2 results in decreased production of cGMP, rapid cGMP breakdown by activated PDE-1 and PDE-2, closure of cGMP channels, and termination of signaling. Note that this speculative model likely omits additional regulatory control.

Disrupting PDE-2 or EGL-4 PKG increases the likelihood that a rise in $[O_2]$ will evoke a fall instead of a rise in [cGMP] in PQR. Like in wild-type animals, this inhibition of cGMP accumulation does not occur if *pde-2* or *egl-4* mutants are also defective in *pde-1* or in CNGC subunits. Thus, one role of PKG and PDE-2 is to control the rise in [cGMP] following a rapid increase in $[O_2]$ to prevent excessive Ca^{2+}-dependent negative feedback. In *pde-1; pde-2* double mutants, [cGMP] is high regardless of $[O_2]$, and changing $[O_2]$ fails to evoke changes in [cGMP], suggesting that these two enzymes account for most or all of the PDE activity in PQR. PDE-2 has several predicted PKG phosphorylation sites through which EGL-4 could stimulate PDE-2 activity (Fig. S4).

O_2-evoked Ca^{2+} signaling in PQR fails in a substantial proportion of wild-type animals, and this proportion increases in *pde-1*, *pde-2* and *egl-4* mutants. Simultaneous Ca^{2+} and cGMP imaging experiments in wild-type animals suggest that Ca^{2+} signaling failure is associated with a lack of measurable cGMP responses in the cell body. The reason for failure is unclear because we cannot yet measure cGMP in the vicinity of the cGMP channel or gating of this channel [the Ca^{2+} we measure reflects downstream activation of the EGL-19 L-type voltage-gated Ca^{2+} channel, and the IP_3 and ryanodine receptors (38)]. One possibility is that failure reflects excessive Ca^{2+}-mediated negative feedback that acts locally and shuts off cGMP signal transduction before the L-type voltage gated Ca^{2+} channels, IP_3, and ryanodine receptors can be activated.

The Ca^{2+} and cGMP responses evoked in PQR when an individual wild-type animal is repeatedly exposed to the same $[O_2]$ stimulus are highly reproducible, suggesting that the cGMP signal transduction mechanism per se is reliable. By contrast, PQR responses to the same $[O_2]$ stimulus vary considerably among wild-type individuals. This interanimal variation was surprising because it occurs across a population of genetically identical animals, grown in the same conditions. A potential explanation for this variation is stochastic differences in the expression of genes that mediate cGMP sensory transduction in PQR. It will be interesting to examine whether these observations can be extended to other sensory neurons and whether they provide insight into the stochastic nature of behavioral responses.

The cGi500 sensor is similar in dynamic range to first-generation Ca^{2+} sensors such as YC2.12 (45). Iterative improvements have led to genetically encoded Ca^{2+} sensors with large signal-to-noise ratios that can be targeted to different subcellular regions such as synapses (46) and ion channels (47). These improvements have led to widespread adoption of these Ca^{2+} sensors in biology. cGMP sensors await similar improvement.

Materials and Methods

C. elegans strains were grown under standard conditions (48). The *db40* allele was isolated in a screen for suppressors of aggregation, mapped to *pde-1*, and confirmed by sequencing and failure to complement *pde-1 (ok2924)*. Imaging was done as described previously (36), except for simultaneous imaging of Ca^{2+} and cGMP, which was done on a spinning disk confocal. For detailed methods, a list of worm strains, and PCR primers, see *SI Materials and Methods*.

ACKNOWLEDGMENTS. We thank I. Rabinowitch, R. S. Branicky, C. Chen, and W. Schafer for reagents; R. Murphy for scripts; K. E. Busch for microfluidic devices; P. Laurent, N. Barry, and J. Howe for help with microscopy; Mei Zhen for providing us with *egl 4* cDNA; M.d.B. and W. Schafer laboratory members for comments and advice; and the *C. elegans* Knockout Consortium, the National BioResource Project (Japan), and the *Caenorhabditis* Genetics Centre for strains. A.C. was supported by the European Molecular Biology

Organization and Medical Research Council Career Development Fellowships. S.O. was supported by the Uehara Memorial Foundation. M.d.B. acknowledges support from an Advanced European Research Council grant (Proposal no. 269058 - ACMO).

1. Fu Y, Yau KW (2007) Phototransduction in mouse rods and cones. *Pflugers Arch* 454(5):805–819.
2. Kleppisch T, Feil R (2009) cGMP signalling in the mammalian brain: Role in synaptic plasticity and behaviour. *Handb Exp Pharmacol* 191:549–579.
3. Xu Y, Zhang HT, O'Donnell JM (2011) Phosphodiesterases in the central nervous system: Implications in mood and cognitive disorders. *Handb Exp Pharmacol* 204:447–485.
4. Nikolaev VO, Lohse MJ (2009) Novel techniques for real-time monitoring of cGMP in living cells. *Handb Exp Pharmacol* 191:229–243.
5. Vincent P, Gervasi N, Zhang J (2008) Real-time monitoring of cyclic nucleotide signaling in neurons using genetically encoded FRET probes. *Brain Cell Biol* 36(1-4): 3–17.
6. Honda A, et al. (2001) Spatiotemporal dynamics of guanosine 3′,5′-cyclic monophosphate revealed by a genetically encoded, fluorescent indicator. *Proc Natl Acad Sci USA* 98(5):2437–2442.
7. Cawley SM, Sawyer CL, Brunelle KF, van der Vliet A, Dostmann WR (2007) Nitric oxide-evoked transient kinetics of cyclic GMP in vascular smooth muscle cells. *Cell Signal* 19(5):1023–1033.
8. Sato M, Nakajima T, Goto M, Umezawa Y (2006) Cell-based indicator to visualize picomolar dynamics of nitric oxide release from living cells. *Anal Chem* 78(24): 8175–8182.
9. Honda A, Moosmeier MA, Dostmann WR (2005) Membrane-permeable cygnets: Rapid cellular internalization of fluorescent cGMP-indicators. *Front Biosci* 10:1290–1301.
10. Shelly M, et al. (2010) Local and long-range reciprocal regulation of cAMP and cGMP in axon/dendrite formation. *Science* 327(5965):547–552.
11. Lucas KA, et al. (2000) Guanylyl cyclases and signaling by cyclic GMP. *Pharmacol Rev* 52(3):375–414.
12. Conti M, Beavo J (2007) Biochemistry and physiology of cyclic nucleotide phosphodiesterases: Essential components in cyclic nucleotide signaling. *Annu Rev Biochem* 76:481–511.
13. Kleppisch T (2009) Phosphodiesterases in the central nervous system. *Handb Exp Pharmacol* 191:71–92.
14. Kuhn M (2009) Function and dysfunction of mammalian membrane guanylyl cyclase receptors: Lessons from genetic mouse models and implications for human diseases. *Handb Exp Pharmacol* 191:47–69.
15. Derbyshire ER, Marletta MA (2012) Structure and regulation of soluble guanylate cyclase. *Annu Rev Biochem* 81:533–559.
16. Francis SH, Blount MA, Corbin JD (2011) Mammalian cyclic nucleotide phosphodiesterases: Molecular mechanisms and physiological functions. *Physiol Rev* 91(2): 651–690.
17. Hofmann F, Bernhard D, Lukowski R, Weinmeister P (2009) cGMP regulated protein kinases (cGK). *Handb Exp Pharmacol* 191:137–162.
18. Reaume CJ, Sokolowski MB (2009) cGMP-dependent protein kinase as a modifier of behaviour. *Handb Exp Pharmacol* 191:423–443.
19. Kaupp UB, Seifert R (2002) Cyclic nucleotide-gated ion channels. *Physiol Rev* 82(3): 769–824.
20. de Bono M, Maricq AV (2005) Neuronal substrates of complex behaviors in C. elegans. *Annu Rev Neurosci* 28:451–501.
21. Coburn CM, Bargmann CI (1996) A putative cyclic nucleotide-gated channel is required for sensory development and function in *C. elegans*. *Neuron* 17(4):695–706.
22. Komatsu H, Mori I, Rhee JS, Akaike N, Ohshima Y (1996) Mutations in a cyclic nucleotide-gated channel lead to abnormal thermosensation and chemosensation in *C. elegans*. *Neuron* 17(4):707–718.
23. Birnby DA, et al. (2000) A transmembrane guanylyl cyclase (DAF-11) and Hsp90 (DAF-21) regulate a common set of chemosensory behaviors in *Caenorhabditis elegans*. *Genetics* 155(1):85–104.
24. L'Etoile ND, et al. (2002) The cyclic GMP-dependent protein kinase EGL-4 regulates olfactory adaptation in C. elegans. *Neuron* 36(6):1079–1089.
25. Wasserman SM, Beverly M, Bell HW, Sengupta P (2011) Regulation of response properties and operating range of the AFD thermosensory neurons by cGMP signaling. *Curr Biol* 21(5):353–362.
26. Ortiz CO, et al. (2006) Searching for neuronal left/right asymmetry: Genomewide analysis of nematode receptor-type guanylyl cyclases. *Genetics* 173(1):131–149.
27. Fujiwara M, Sengupta P, McIntire SL (2002) Regulation of body size and behavioral state of C. elegans by sensory perception and the EGL-4 cGMP-dependent protein kinase. *Neuron* 36(6):1091–1102.
28. Stansberry J, et al. (2001) A cGMP-dependent protein kinase is implicated in wild-type motility in C. elegans. *J Neurochem* 76(4):1177–1187.
29. Komatsu H, et al. (1999) Functional reconstitution of a heteromeric cyclic nucleotide-gated channel of *Caenorhabditis elegans* in cultured cells. *Brain Res* 821(1):160–168.
30. Cho SW, Choi KY, Park CS (2004) A new putative cyclic nucleotide-gated channel gene, cng-3, is critical for thermotolerance in Caenorhabditis elegans. *Biochem Biophys Res Commun* 325:525–531.
31. Cho SW, Cho JH, Song HO, Park CS (2005) Identification and characterization of a putative cyclic nucleotide-gated channel, CNG-1, in C. elegans. *Mol Cells* 19:149–154.
32. Nikolaev VO, Gambaryan S, Lohse MJ (2006) Fluorescent sensors for rapid monitoring of intracellular cGMP. *Nat Methods* 3(1):23–25.
33. Russwurm M, et al. (2007) Design of fluorescence resonance energy transfer (FRET)-based cGMP indicators: A systematic approach. *Biochem J* 407(1):69–77.
34. Cheung BH, Cohen M, Rogers C, Albayram O, de Bono M (2005) Experience-dependent modulation of C. elegans behavior by ambient oxygen. *Curr Biol* 15(10): 905–917.
35. Gray JM, et al. (2004) Oxygen sensation and social feeding mediated by a *C. elegans* guanylate cyclase homologue. *Nature* 430(6997):317–322.
36. Persson A, et al. (2009) Natural variation in a neural globin tunes oxygen sensing in wild Caenorhabditis elegans. *Nature* 458(7241):1030–1033.
37. Zimmer M, et al. (2009) Neurons detect increases and decreases in oxygen levels using distinct guanylate cyclases. *Neuron* 61(6):865–879.
38. Busch KE, et al. (2012) Tonic signaling from O_2 sensors sets neural circuit activity and behavioral state. *Nat Neurosci* 15(4):581–591.
39. Richmond JE, Davis WS, Jorgensen EM (1999) UNC-13 is required for synaptic vesicle fusion in C. elegans. *Nat Neurosci* 2(11):959–964.
40. Zhao Y, et al. (2011) An expanded palette of genetically encoded Ca^{2+} indicators. *Science* 333(6051):1888–1891.
41. Xu RX, et al. (2000) Atomic structure of PDE4: Insights into phosphodiesterase mechanism and specificity. *Science* 288(5472):1822–1825.
42. Shen X, et al. (2008) Ca(2+)/Calmodulin-binding proteins from the C. elegans proteome. *Cell Calcium* 43(5):444–456.
43. Cheung BH, Arellano-Carbajal F, Rybicki I, de Bono M (2004) Soluble guanylate cyclases act in neurons exposed to the body fluid to promote *C. elegans* aggregation behavior. *Curr Biol* 14(12):1105–1111.
44. Arellano-Carbajal F, et al. (2011) Macoilin, a conserved nervous system-specific ER membrane protein that regulates neuronal excitability. *PLoS Genet* 7(3):e1001341.
45. Miyawaki A, et al. (1997) Fluorescent indicators for Ca2+ based on green fluorescent proteins and calmodulin. *Nature* 388(6645):882–887.
46. Dreosti E, Odermatt B, Dorostkar MM, Lagnado L (2009) A genetically encoded reporter of synaptic activity in vivo. *Nat Methods* 6(12):883–889.
47. Tay LH, et al. (2012) Nanodomain Ca^{2+} of Ca^{2+} channels detected by a tethered genetically encoded Ca^{2+} sensor. *Nat Commun* 3:778.
48. Sulston J, Hodgkin J (1988) *The Nematode Caenorhabditis elegans*, ed Wood WB (CSHL Press, Cold Spring Harbor), pp 587–606.